Journal of Computer Assisted Tomography
17(2):173–177, March/April

3D Phase Contrast MRI of Cerebral Blood Flow and Surface Anatomy

Harvey E. Cline, William E. Lorensen, and William J. Schroeder

Abstract: Noninvasive MR acquisition of blood flow and stationary tissue provides three-dimensional display of flow and of the vascular and brain surfaces. The calculated motion of a simulated bolus injection is derived from the measured velocity vector field and is animated to resemble cine angiography. Simulation of a bolus injection into the basilar artery of a healthy volunteer shows the blood flow into the posterior cerebral arteries. **Index Terms:** Blood, flow dynamics — Brain, anatomy — Magnetic resonance imaging, three-dimensional.

Angiographic studies are included in ~10% of today's clinical MR examinations. Over the past decade, there has been a dramatic increase in fine vessel resolution with stationary tissue suppression due to improved acquisition technique and instrumentation (1–14). Although magnetic resonance angiography (MRA) has not yet replaced the more invasive X-ray angiography, it does provide valuable information to assess vascular flow. New three-dimensional (3D) PC techniques provide both stationary tissue contrast and a blood velocity vector field from a single acquisition. However, it is not easy to visualize the anatomy and analyze the blood flow from this vast amount of data. At present the flow information is stored as velocity component images that are difficult to analyze. We have designed a 3D model and have simulated a bolus injection from a 3D simultaneous PC angiography acquisition to provide more information for surgical planning and for the diagnosis of vascular pathology.

Magnetic resonance contrast depends on both the dynamics of precessing nuclear spins and relaxation phenomena. Flow contrast is provided by either time-of-flight (TOF) (3,5,7,9–12,14) or PC (1,2,9–13) pulse sequences. In the TOF methods (8) the magnitude of the spin signal is influenced by the flow. In the PC methods (6) the phase of the nuclear spins is detected with a flow encoding bipolar gradient pulse. Motion of nuclear spins in a magnetic field gradient induces a change in magnetization or a phase shift.

Phase contrast pulse sequences provide simultaneous 3D contrast of the stationary tissue and a quantitative blood velocity vector field (13), and with a maximum intensity projection MRA can be performed (11,15). The surfaces of the blood vessels have been constructed from 3D TOF MRA (16), and 3D surfaces of the brain have been displayed from MRA using connectivity (17–20) or multispectral analysis (21–23). Both the surfaces of the brain and those of the blood vessels have been integrated into a single 3D model for surgical planning (23). The brain anatomy and the blood flow surface can be derived from a single 3D acquisition (13,23). For surgical planning applications, one desires a safe trajectory from the entry point to the target that does not intersect blood vessels (22,23). Although TOF acquisitions are usually faster than PC methods for creating MRA, they require an additional registered stationary tissue acquisition to construct a 3D model for surgical planning.

We demonstrate blood flow patterns using a simulated bolus injected into a 3D model derived from PC MR data. A surface model is constructed, markers are placed in the arteries to simulate a bolus of dye, and the motion of the bolus is derived from the fluid velocity.

MATERIALS AND METHODS

Magnetic Resonance Acquisition

The heads of three healthy volunteers were scanned with 1.5 T MR systems (GE Medical Sys-

From GE Corporate Research and Development, Building K1, Room 1C32, P.O. Box 8, Schenectady, NY 12301, U.S.A. **Address correspondence and reprint requests to Dr. H. E. Cline.**

tems, Milwaukee, WI, U.S.A.). Dumoulin et al. (13) acquired 128 slices 1.8 mm thick in ~1 h with their research pulse sequence, 256 x 256 resolution, 24 cm field-of-view (FOV), 20" flip angle, an echo time (TE) of 11 ms, and repetition time (TR) of 30 ms. In clinical practice a smaller data set is acquired in less time. A second data set of 60 axial slices 0.8 mm thick near the base of the brain was acquired in 15 min with a 20 cm FOV using a product pulse sequence with the following parameters: TR 26 ms, TE 7.6 ms, 20° flip angle, and 256 × 128 resolution. Five sets of images were reconstructed from a single acquisition with the following displays: a: stationary tissue; b: blood speed; c: x, velocity; d: y, velocity; and e: z, velocity (Fig. 1). The third data set was acquired in 20 min at a clinical site (Brigham and Women's Hospital, Boston, MA, U.S.A.) using 28 coronal slices 1 mm thick covering the carotid arteries, with a 20 cm FOV, 20" flip angle, and 256 × 192 resolution.

The stationary tissue images show the brain with bright blood vessels, whereas the flow speed images display only the moving blood with an intensity proportional to the speed. Surface images of the blood vessels were constructed from flow data with the dividing cubes algorithm using connectivity to suppress unconnected noise (16). However, connectivity alone could not be used with stationary tissue magnitude images to isolate the brain surface from the vessel surfaces. Rather, two sets of 3D images (stationary and speed) were needed and processed with a multispectral segmentation method to separate the brain and blood vessel voxels (23). A brain surface was generated from the segmented data and displayed with the blood vessel surface using the dividing cubes algorithm (19).

A 3D model of the blood vessels (red) and brain surface (gray) was constructed and rendered at different orientations (Fig. 2a). Such models have been used to plan surgery since the surgeons need to locate blood vessels in three dimensions. Sections through the brain are made to view the internal blood vessels (Fig. 2b).

Simulated Bolus Injection

To illustrate the feature of a simulated bolus injection, the basilar artery was selected because it bifurcates into the left and right posterior cerebral arteries. A simulated bolus injection was created from the second 60 slice vascular study at the base of the brain. Transparent blood vessel surfaces derived from flow magnitude data were rendered with the marching cubes algorithm (18). A number of simulated small seeds were placed at the entry of the basilar artery to mimic a bolus injection. During the continuous simulated injection, seeds were created with small random displacements across the vessel cross section at the artery entrance. The displacement $\mathbf{dr}_i$ of each seed was calculated from the steady state velocity vector V_i after each time step dt by

$$\mathbf{dr}_i = V_i \, \mathrm{dt}$$

The velocity V_i is an average velocity at point i measured throughout the acquisition; however, V_i does not include the periodic cardiac motion. At each time step, the simulated markers were displaced. After 20 steps, the image of the transparent vessels and of the markers was recorded on video tape. There were 20 integration steps for each frame and each frame represented 0.0017 s of actual time. Playback of the resulting sequence of images at 30 frames/s shows the blood flow pattern and the injected bolus movement. After the injection, the vir-

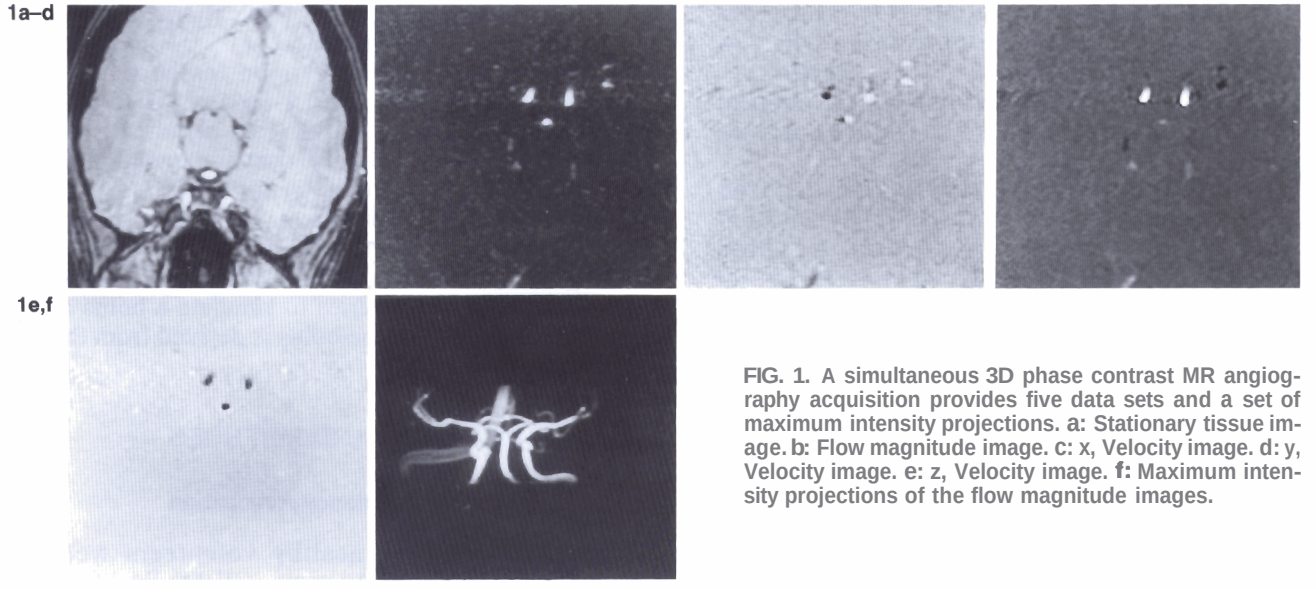

FIG. 1. A simultaneous 3D phase contrast MR angiography acquisition provides five data sets and a set of maximum intensity projections. a: Stationary tissue image. b: Flow magnitude image. c: x, Velocity image. d: y, Velocity image. e: z, Velocity image. f: Maximum intensity projections of the flow magnitude images.

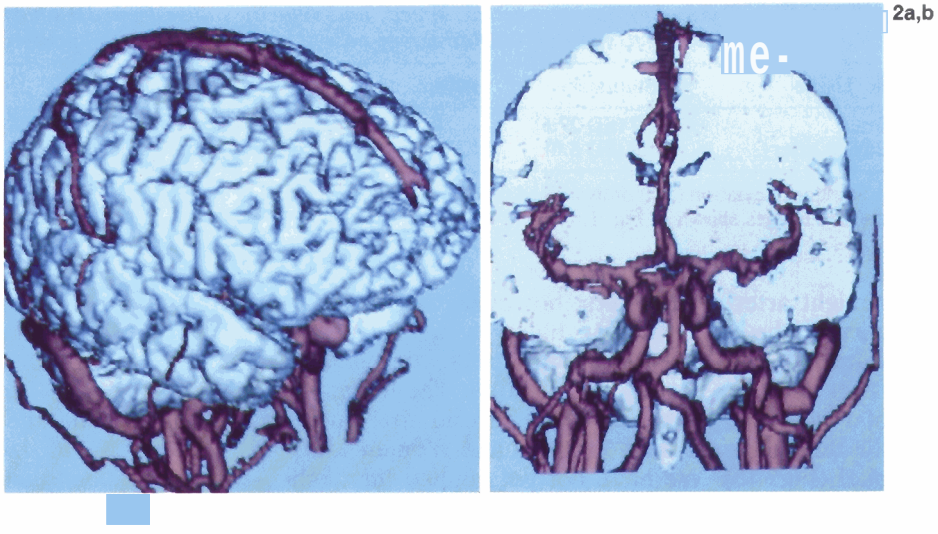

FIG. 2. The brain and vascular surfaces are constructed from 128 axial slices covering a 24 cm cube using a simultaneous 3D phase contrast acquisition developed by Dumoulin et al. (13) of both stationary tissue and blood flow speed images, a: Lateral oblique view of the brain (gray) and blood vessel (red) surfaces constructed with the dividing cubes algorithm. **b:** Coronal brain cut to view the basilar and deep cerebral arteries.

tual bubbles move through the artery marking the blood flow. This representation is often used in fluid flow visualization experiments where actual bubbles of hydrogen mark the flow.

RESULTS

A bolus was simulated at the entrance of the basilar artery, and the markers migrated through the bifurcation to enter both posterior cerebral arteries. The animation of a simulated bolus of bubbles moving through the blood vessels resembles cine angiography (Fig. 3). This motion is best shown by viewing a cine loop of the calculated bolus. The transparent vessels calculated at a constant speed surface are superimposed to show the position of the vessels. Some of the markers appear to move outside the speed surface, which is interior to the actual vessel wall.

The voxel intensities and measured velocities in the region of the bifurcation are listed in Table 1. The standard deviation SD indicates the scatter of the data for the images shown in Fig. I. The stationary tissue appears to drift at a slow velocity due to errors, which, if desired, could be corrected, in reconstructing the velocity data.

Blood flow through healthy arteries in the head shows a laminar flow pattern with some circulation at the level of the curvatures of the vessels. The flow in the carotid arteries was demonstrated with an animated sequence of migrating spherical markers derived from the velocity field. The distribution of spherical markers is shown in the carotid artery (Fig. 4a). Blood flow is most rapid in the center of

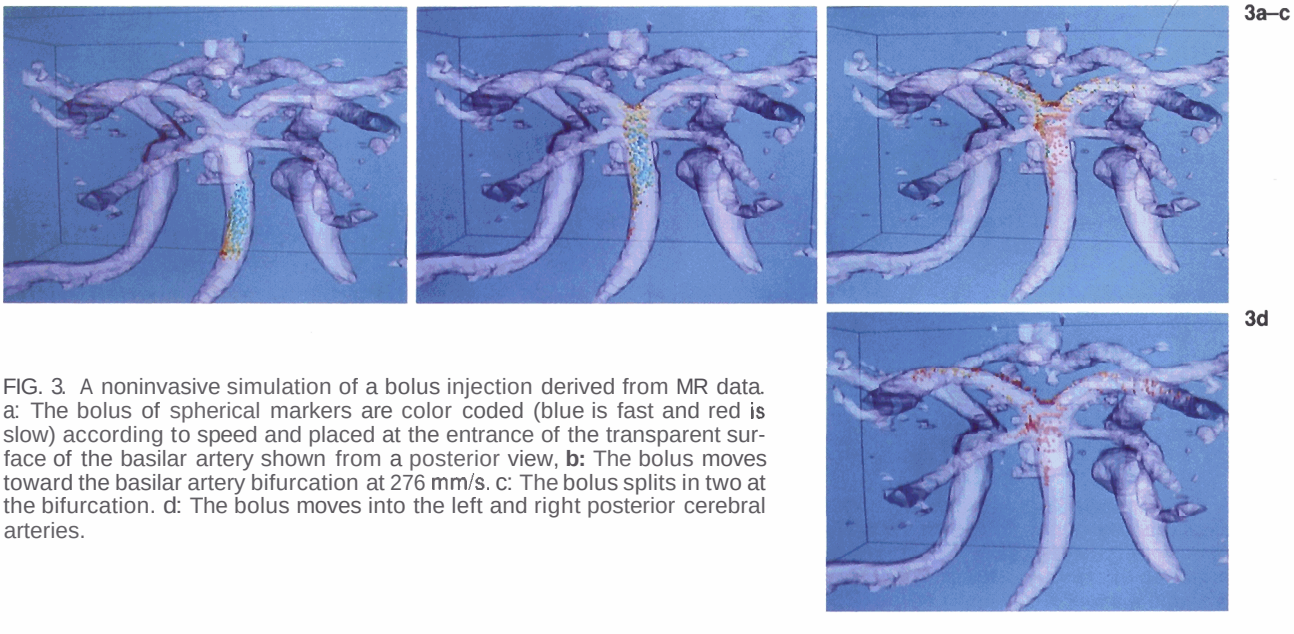

FIG. 3. A noninvasive simulation of a bolus injection derived from MR data. a: The bolus of spherical markers are color coded (blue is fast and red is slow) according to speed and placed at the entrance of the transparent surface of the basilar artery shown from a posterior view, **b:** The bolus moves toward the basilar artery bifurcation at 276 mm/s. c: The bolus splits in two at the bifurcation. d: The bolus moves into the left and right posterior cerebral arteries.

TABLE 1. Stationary tissue contrast, speed, and velocity values from 3D phase contrast MR angiography in the brain tissue and basilar artery near the bifurcation of the posterior cerebral arteries

Tissue	Stationary	Speed (mm/s)	V_x (mm/s)	V_y (mm/s)	V_z (mm/s)
Brain	82.7 (SD 27.6)	43.7 (SD 16.5)	– 3.4 (SD 28.2)	– 1.3 (SD 26.2)	6.1 (SD 31.6)
Basilar artery	480.8 (SD 8.0)	275.6 (SD 52.0)	1.9 (SD 65.2)	83.9 (SD 10.6)	– 251.9 (SD 56.9)

Standard deviation (SD) of measured pixel intensities was calculated in both the basilar artery and brain region of interest on each of the five images shown in Fig. 1.

straight arterial segments; however, as the vessel curves, the rapid flowing blood is displaced outward by centrifugal force and a circulation pattern is set up in the vessel cross section. The trajectory of a marker is calculated in the carotid artery using the third data set from Brigham and Women's hospital (Fig. 4b). We have not yet applied this technique to diseased vessels where it is likely that flow will be perturbed.

There are several limitations to the flow visualization technique described above. The PC MR acquisition averages blood flow over minutes, and the resulting velocity field does not include the contribution of periodic cardiac motion. Thus, the periodic motion of the particles in the bolus is not shown in the simulation. A much faster acquisition sequence would be required to show the periodic cardiac fluid motion. Since the velocity is deduced from the phase of the spins, there is a maximum velocity that may be detected at a phase of π. The velocity sensitivity may be set by the flow encoding bipolar gradient strength. Regions of high flow near narrowed vessels may give a low flow signal from phase wrap or phase dispersion within a voxel. Random background noise in the velocity field causes the simulated marker to undergo a random walk as the marker migrates up the artery at a time averaged velocity, V. The random component of the velocity may add or subtract from the actual velocity, but the random component adds to the square displacement ε_n^2 after n jumps of distance to give 6 (24)

$$\varepsilon_n^2 = n\delta^2$$

Assuming that the marker jumps each time it enters a new voxel of size s, the number of jumps depends on the velocity and time by $n = Vt/s$.

The size of the average jump 6 depends on the voxel size s, the velocity signal V, and the noise a by $6 = \sigma s/V$. The displacement error after a time t is given by

$$\varepsilon_n = \sqrt{n}\,\frac{\sigma}{V}s$$

In the example shown in Fig. 2, the velocity V is 276 mmls, the background velocity components standard deviation (SD) is approximately $a = 30$ mm/s, the voxel size is $s = 0.8$ mm, and with $n = 40$ jumps in the basilar artery from the entrance to the bifurcation the estimated random walk error is $\varepsilon_n = 0.6$ mm. During a 0.12s time of migration, the displacement from a 4 mm/s drift velocity normal to the vessel becomes only 0.4 mm. In this case both random and systematic velocity errors create a displacement of less than a voxel size.

In the future a comparison between healthy and diseased vessels would provide a measure of the clinical utility of this technique. Furthermore to validate the technique, the simulated bolus tracking needs to be compared in the same subject with actual X-ray bolus tracking.

4a,b

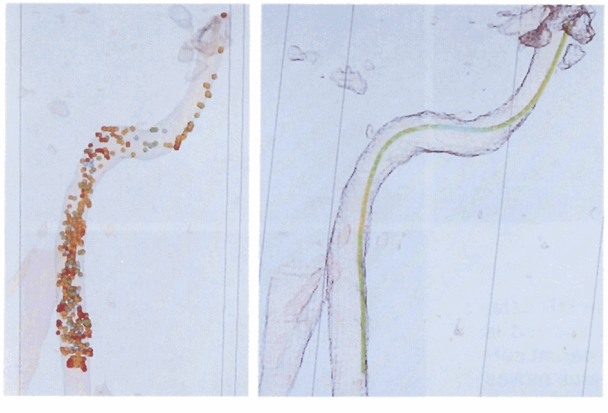

FIG. 4. A simulated bolus of spherical markers injected into a carotid artery of the third data set consists of 28 coronal slices 1 mm thick (Brigham and Women's Hospital). **a:** The distribution of markers in the carotid artery. **b:** The trajectory of a single marker.

CONCLUSION

The idea of simulating a cine angiography bolus injection with MR derived flow data simplifies the flow analysis by replacing 3D blood flow vector fields with simple animation. Angiography injects virtual bubbles to view the flow. A model of blood vessels and brain surface provides the surgeon with information about deep vessels lacking in projection displays.

Acknowledgment: The authors acknowledge C. L. Dumoulin, S. P. Souza, and R. D. Darrow of our laboratory; R. Kikinis of Brigham and Women's Hospital, Boston, MA; and D. Sherill, M. Bernstein, and T. Kennedy of GE Medical Systems, Milwaukee, WI, for stimulating discussions and providing 3D PC angiography data sets.

REFERENCES

1. Hahn EL. Detection of sea-water motion by nuclear precession. J *Geophys Res* 1960;65:776–80.
2. Wedeen VJ, Mueli RA, Edelman RR, et al. Projective imaging of pulsatile flow with magnetic resonance. *Science* 1985; 230:946–8.
3. Wehrli FW, Suimakawa A, MacFall JR, Axel L, Perman W. MR imaging of venous and arterial flow by a selective saturation-recovery spin echo (SSRSE) method. J *Comput Assist Tomogr* 1985;9:537–45.
4. Axel L, Morton D. A method for imaging blood vessels by phase compensatedluncompensated difference images. *Magn Reson Imaging* 1986;4:153–00.
5. Dixon WT, Du LN, Faul DD, Gado M, Rossnick S. Projection angiograms of blood labelled by adiabatic fast passage. *Magn Reson Med* 1986;3:454–62.
6. Dumoulin CL, Hart HR. Magnetic resonance angiography. *Radiology* 1986;161:717–20.
7. Dumoulin CL, Cline HE, Souza SP, Wagle WA, Walker MF. Three-dimensional time-of-flight magnetic resonance angiography using spin saturation. *Magn Reson Med* 1989; 11:35–46.
8. Dumoulin CL, Souza SP, Walker MF, Wagle WA. Three-dimensional phase contrast angiography. *Magn Reson Med* 1989;9:139–49.
9. Keller PJ, Drayer BP, Fram EK, et al. MR angiography with two-dimensional acquisition and three-dimensional display. *Radiology* 1989;173:527–32.
10. Nishimura DG, Macovski A, Pauly JM. Considerations of magnetic resonance angiography by selective inversion recovery. *Magn Reson Med* 1989;7:472–84.
11. Ruggieri PM, Laub GA, Masaryk TJ, Modic MT. Intercranial circulation: pulse sequence considerations in three-dimensional (volume) MR angiography. *Radiology* 1989;171: 785–91.
12. Singer JR. Blood flow rates by nuclear magnetic resonance measurements. *Science* 1959;130:1652–3.
13. Dumoulin CL, Souza SP, Darrow RD, Pelc N, Ash SA. Simultaneous acquisition of phase-contrast angiograms and stationary-tissue images with Hadamard encoding of flow-induced phase shifts. J *Magn Res Imaging* 1991;1:399–00.
14. Parker DL, Yuan C, Blatter DD. MR angiography by multiple thin slab 3D acquisition. *Magn Reson Med* 1991;17: 434–51.
15. Cline HE, Dumoulin CL, Lorensen WE, Souza SP, Adams WJ. Volume rendering connectivity algorithms for MR angiography. *Magn Reson Med* 1991;18:384–94.
16. Cline HE, Lorensen WE, Herfkens RJ, Johnson GA, Glover GH. Vascular morphology by three-dimensional magnetic resonance imaging. *Magn Reson Imaging* 1989;7:45–54.
17. Cline HE, Dumoulin CL, Hart HR Jr, Lorensen WE, Ludke S. 3D reconstruction of the brain from magnetic resonance images using a connectivity algorithm. *Magn Res Imaging* 1987;5:345–52.
18. Lorensen WE, Cline HE. Marching cubes: a high resolution surface construction algorithm. *Comput Graphics* 1987;21: 163–8.
19. Cline HE, Lorensen WE, Ludke S, Crawford CR, Teeter BC. Two algorithms for the three-dimensional reconstruction of tomograms. *Med Phys* 1989;15:320–7.
20. Levin DN, Hu X, Tan KK, Galhotra S. Surface of the brain: three-dimensional MR images created with volume rendering. *Radiology* 1989;171:277–80.
21. Vannier MW, Butterfield RL, Jordan D, et al. Multispectral analysis of magnetic resonance images. *Radiology* 1985;154: 221–4.
22. Cline HE, Lorensen WE, Kikinis R, Jolesz F. Technical note. Three-dimensional segmentation of MR images of the head using probability and connectivity. J *Comput Assist Tomogr* 1990;14:1037–45.
23. Cline HE, Lorensen WE, Souza SP, et al. Technical note. 3D surface rendered MR images of the brain and its vasculature. J *Comput Assist Tomogr* 1991;15:344–51.
24. Feynman RP, Leighton RB, Sands M. *The Feynman lectures on physics, Vol I*. Addison-Wesley, MA 1963.